Ultrasonics Sonochemistry 88 (2022) 106106

Contents lists available at ScienceDirect

Ultrasonics Sonochemistry

journal homepage: www.elsevier.com/locate/ultson

Effective removal of organics from Bayer liquor through combined sonolysis and ozonation: Kinetics and mechanism

Jianfeng Ran [a,b], Haisheng Duan [a,b,c], C. Srinivasakannan [d], Jiashu Yao [a,b], Shaohua Yin [a,b,*], Libo Zhang [a,b,*]

[a] Faculty of Metallurgical and Energy Engineering, Kunming University of Science and Technology, Kunming, Yunnan 650093, China
[b] State Key Laboratory of Complex Nonferrous Metal Resources Clean Utilization, Kunming University of Science and Technology, Kunming, Yunnan 650093, China
[c] Yunnan Wenshan Aluminum Co., Ltd., Wenshan, Yunnan 663000, China
[d] Chemical Engineering Department, Khalifa University of Science and Technology, Abu Dhabi, United Arab Emirates

ARTICLE INFO

Keywords:
Organics
Bayer liquor
Sonolysis
Ozonation
US/O_3
AOPs

ABSTRACT

The presence of organic compounds in the waste liquor is of serious environmental concern that has plagued the development of alumina industry (Bayer Process). The present work attempts to develop a green and efficient process for removal of organics utilizing combined effect of sonolysis and ozonation (US/O_3). The effects of reaction duration, ozone concentration and ultrasonic power are assessed for sonolysis (US), ozonation (O_3) and combination of sonolysis and ozonation (US/O_3). The optimal conditions for US/O_3 treatment system is identified to be a reaction duration of 7 h, ozone concentration of 7.65 g/h, and ultrasonic power of 600 W. The total organic carbon (TOC) removal and decolorization are 60.13% and 87.1%, respectively. The process can be scaled-up to industrial scale, which could potentially serve to be a convenient, safe and sustainable alternative to the exisiting treatment technologies. Additionally, the treated waste water can be reused contributing to an improvement in the overall economics.

1. Introduction

Aluminum is the third most abundant element in the Earth's crust [1]. Aluminum alloyed with other metals has innumerable applications ranging from aerospace industry to food packaging. Aluminum is produced by the electrolytic reduction of alumina (Al_2O_3), utilizing Bayer process which has four main process stages: (i) dissolution of bauxite using strong alkaline at a pressure of 0.5 MPa, at a temperature of 270–300 °C, (ii) addition of seed crystal to facilitate crystallization of aluminum hydroxide, (iii) calcination of aluminum hydroxide to Al_2O_3, and (iv) evaporation of spent liquor [2,3]. As a result, bauxite is digested in a highly caustic solution and thus forms a hot sodium aluminate solution (i.e. Bayer liquor).

However, presence of organic compounds in Bayer liquor is one of the biggest challenges facing the aluminium industries. The major source of organics in the waste liquor is from bauxite (96%), while the other organic matters are due to the addition of flotation agents, flocculants, etc. [4]. The presence of organic contaminants contribute to the reduction in quality and yield of alumina products. Accumulation of organic compounds in the process is known to cause many problems which include alumina yield reduction, darken the color of solution, dull the color of alumina, excessive generation of fine gibbsite particles, lower sedimentation rate of red mud, increase impurities in alumina and increase caustic loss, density, viscosity and boiling point, etc. [5–7]. On the other hand, discharge of such organic pollutants will violate the environmental regulations in particular total organic carbon (TOC) level that may cause lack of dissolved oxygen in the water, leading to putrefaction and fermentation, anaerobic bacterial growth, etc., affecting the flora and fauna of the water bodies.

The technologies that are in practice to deal with the organic matter in Bayer liquor, include bauxite roasting, mother liquor roasting, ion exchange, crystallization, lime causticization and wet oxidation, each with specific merits and demerits. Bauxite roasting are energy intensive and generate serious gaseous discharges [8]; the mother liquor roasting are energy intensive and corrosive [9]; the ion exchange are not economical due to the high cost of resin and its regeneration [10]; the crystallization are energy intensive with incomplete removal of organic matter [11]; the lime causticization cause low utilization of lime and loss

* Corresponding authors at: Faculty of Metallurgical and Energy Engineering, Kunming University of Science and Technology, Kunming, Yunnan 650093, China.
E-mail addresses: yinsh@kust.edu.cn (S. Yin), zhanglibopaper@126.com (L. Zhang).

https://doi.org/10.1016/j.ultsonch.2022.106106
Received 30 April 2022; Received in revised form 21 June 2022; Accepted 26 July 2022
Available online 29 July 2022

Table 1
Composition and characteristics of Bayer liquor used for the experimental.

Component	N_T	N_C	N_K	Al_2O_3	α_k	N_C/N_T	pH	TOC	$C_{oxalate}$
Concentration (g/L)	179.6	12.2	167.4	102.07	2.7	6.79	14.4	7.925	1.37

Note: N_T: total alkali (Na_2O_T), represents the sum of alkali in the form of Na_2O_K and Na_2O_C in Bayer liquor, g/L; N_C: carbonate alkali (Na_2O_C), represents the alkali existing in the form of Na_2CO_3, calculated as Na_2O, g/L; N_K: caustic alkali (Na_2O_K), represents the alkali in the form of sodium aluminate and NaOH in Bayer liquor, calculated as Na_2O, g/L; Al_2O_3: the mass concentration of Al_2O_3 in Bayer liquor, g/L; α_k: caustic ratio, represents the ratio of caustic to alumina molecular concentration in Bayer liquor; N_C/N_T: the mass percentage of alkali carbonate and total alkali, %; TOC: the total amount of organic matter in Bayer liquor, g/L; $C_{oxalate}$: the Total amount of oxalate in Bayer liquor, g/L.

of aluminum [12]; the wet oxidation demands harsh oxidation conditions that demand capital intensive equipments [1].

Among the different technologies, advanced oxidation processes (AOPs) are recognized as the most effective methods to decompose and mineralize organic pollutants. The most important oxidative route is the non-selective oxidation of organic compounds through the formation of hydroxyl radicals ($^{\bullet}OH$) with high oxidation potential (EOP = 2.8 V) [13–15]. AOPs including ozone oxidation [3], wet oxidation process [16,17], photocatalytic oxidation [18], electrocatalytic oxidation [19], biodegradation method [20], ultrasonic oxidation [21], supercritical water oxidation [22], Fenton oxidation process [23], and other combinations of AOPs [24–26], have been well studied. The literature shows that ozone (O_3) has strong oxidizing properties and is widely used in the degradation of organic matter [27,28]. In addition, ozone oxidation can be considered advantageous since it is produced in situ and does not generate secondary pollution [29]. However, ozone generation is energy intensive, having slow rate of mass transfer. Various methods have appeared to solve this problem, such as $TiO_2/UV/O_3/H_2O_2$ [30,31].

In order to improve the mass transfer rate and solubility of ozone, ultrasonic (US), have also been used to augment ozone for the destruction of organic pollutants in water. US refers to a vibration wave with a frequency higher than 20 kHz, which uses liquid as a medium to propagate around. The action of ultrasonic is mainly due to the cavitation effect, manifested as follows: at high ultrasonic energy, the attractive forces of adjacent liquid phase molecules are broken, forming a cavitation nucleus. And the extremely short lifetime (<10 μs) makes the cavitation nucleus extremely explosive. At the moment of explosion, it can generate a local high temperature and high pressure environment of 4200–5000 K and 20–50 MPa, and produce a microjet with a strong impact at a speed of about 110 m/s [32,33]. Several studies have shown that the hybrid process, compared to cavitation and other AOPs, has advantages in its ability to effectively degrade persistent pollutants and reduce process time, thereby reducing overall energy and oxidant consumption [34–36]. Therefore, US/O_3 can maximize their respective advantages contributing to the removal of organic pollutants more quickly and efficiently. Guo et al. have confirmed that the addition of ultrasonic increases the efficiency of SMX removal by ozonation by 26%, and it is found that ultrasonic can enhance the cleavage of S—N bond, making SMX more vulnerable to being attacked by ozone, thus increasing the removal rate [37]. Cui et al. have studied the oxidative removal of tannic acid (TA) and humic acid (HA) by US/O_3, and reported that the proportion of molecular weight >2000 Da in HA and TA rapidly decreased from 89.53 to 4%, after 0.5 h; confirming the synergistic effect of US and O_3 [38].

Although AOPs are found to have beneficial effects on different organic compounds, the potential and ability of the combined US/O_3 process with reference to the alumina production process has not been reported. In the present study, the Bayer liquor is subjected to oxidation using US, O_3, and combination of US/O_3 systems to assess the effects of reaction duration, ozone concentration and ultrasonic power. Further, efforts are made to understand the mechanism of organics degradation.

2. Materials and methods

2.1. Materials

The Bayer liquor is supplied by Yunnan Wenshan Aluminum Co., ltd., which is collected after evaporating the mother liquor and decomposing the seed crystals. Table 1 shows the composition and the characteristics of Bayer liquor. All reagents used in the experimental procedure are of analytical grade.

2.2. Apparatus and operating conditions

A schematic of the experimental setup is shown in Fig. 1. The system consists of the Bayer liquor, ozone generator, ultrasonic device, thermostat water bath, condenser, and drechsel trap (equipped with 20% KI solution). The ozone generator (JW-30A, Xuzhou Jiuzhoulong Ozone Equipment Manufacturing Co., ltd., China) relies on high-voltage discharge to decompose oxygen molecules in the external air flow to

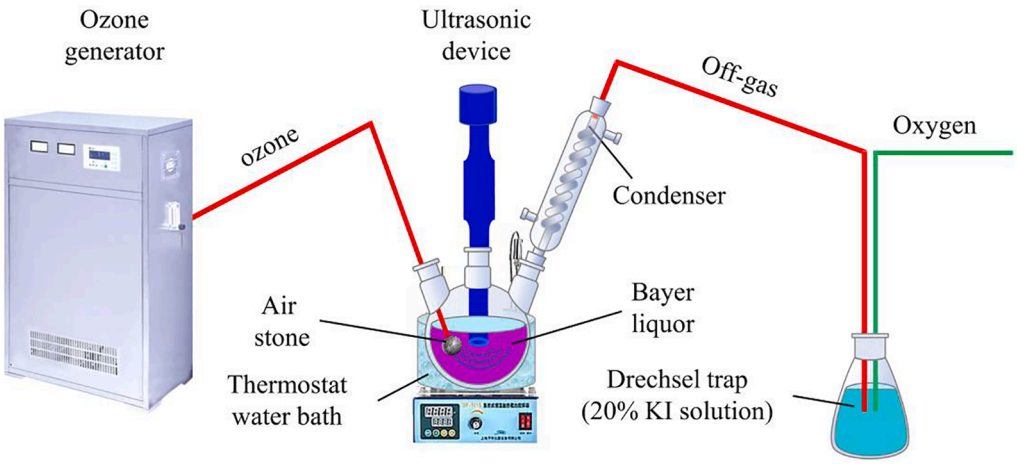

Fig. 1. Schematic of the experimental setup for US/O_3 treatment of organics in Bayer liquor.

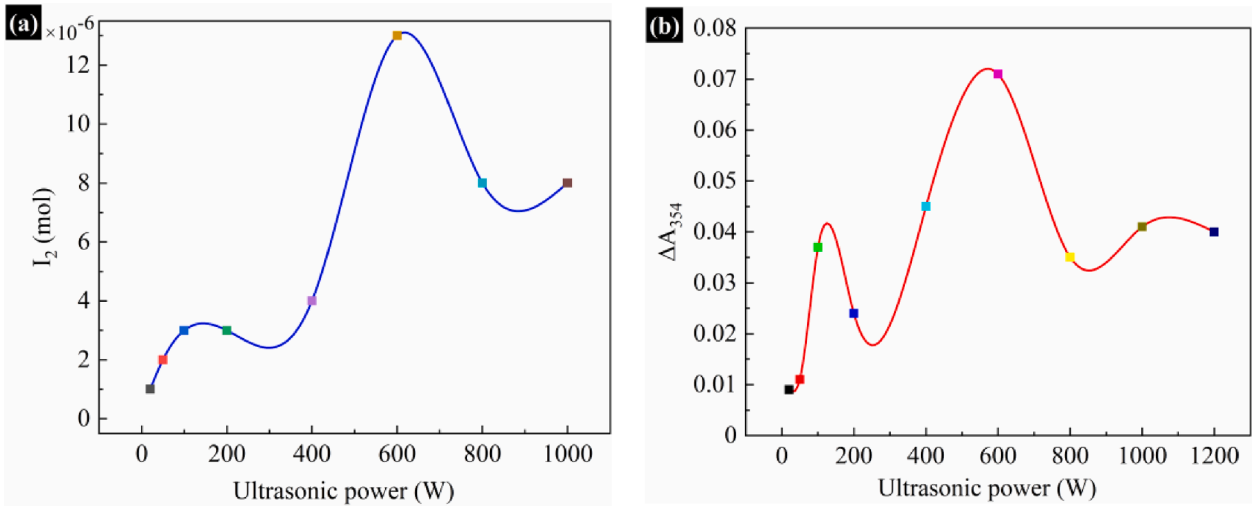

Fig. 2. (a) Relationship between ultrasonic power and iodine release; (b) Relationship between ultrasonic power and ΔA_{354} of potassium iodide solution.

generate ozone of the required concentration (i.e. 2.68, 5.24, 7.65 g/h). The ultrasonic device (2.0 kW, 25 kHz, WM-2000 T, Nanjing Yimaneili Instrument Equipment Co., ltd., China), utilizes a titanium alloy tip placed about 3 cm below the solution interface to diffuse ultrasonic generated at different ultrasonic powers (i.e. 200, 400, 600, 800, 1000 W). In order to match the commercial process conditions, experiments are conducted at 55 °C. The experimental duration is varied from 1 to 10 h to assess the degradation of organics. The sample of volume 10 mL is collected every 1 h to detection analysis during the duration of experiments, and the residual ozone in the off-gas is absorbed using 20% KI solution.

2.3. Analytical methods

The ozone concentration is determined by iodometric method [3]. Ozone is bubbled into the 2 wt% KI solution as described in Eq. (1), and a few drops of 6 mol/L H_2SO_4 are rapidly added to prevent the self-decomposition of ozone. The final solution is titrated with $Na_2S_2O_3$ solution, and starch is selected as a suitable indicator. Eq. (2) is used to calculate the ozone concentration (g/h), where V_1 is the volume of $Na_2S_2O_3$ solution titrated (mL), N is the concentration of $Na_2S_2O_3$ solution titrated (mol/L), M_{O3} is the ozone molecular weight (g/mol), T is ozonation duration (min).

$$2KI + O_3 + H_2O \leftrightarrow I_2 + O_2 + KOH \tag{1}$$

$$C(O_3) = \frac{V_1 \times N \times M_{O_3} \times 60}{T^2 \times 1000} \tag{2}$$

The TOC content and oxalate content of the samples are detected by the carbon–sulfur analyzer (COREY-200, Deyang Kerui Instrument Equipment Factory, China) and the ion chromatography analyzer (Eco IC, Metrohm, Switzerland), respectively. The sample is acidified with 6 mol/L hydrochloric acid (HCl), to discharge inorganic carbon in the form of carbon dioxide (CO_2). Further the pH is reduced below 2, and boiled for about 2 min, to ensure complete removal of inorganic carbon. The treated sample is dried in an oven and its TOC content is measured using carbon–sulfur analyzer. The absorbance spectra of each sample is measured by a ultraviolet and visible spectrophotometer (UV–Vis, UV-2600, Shimadzu, Japan) at wavelengths from 200 to 800 nm, using quartz cells 5 cm long. The % decolorization is measured by the change in the absorbance of the sample at a specific wavelength, as shown in Eq. (3).

$$\%\ Decolorization = \frac{A_{346} - A_{346}'}{A_{346}} \times 100\% \tag{3}$$

where A_{346} and $A_{346'}$ represent the absorbance at 346 nm of the initial and the treated sample, respectively. The three-dimensional fluorescence spectrum analysis, also known as excitation emission matrix spectroscopy (EEMS), is performed utilizing fluorescence spectrophotometer (RF6000, Shimadzu, Japan) at an excitation and emission wavelength and in the range of 350–800 nm and 450–800 nm, respectively. Electron paramagnetic resonance spectroscopy (EPR, A300, Bruker, Germany) is used to detect the main free radicals in the samples, with 5,5-dimethyl-1-pyrroline *N*-oxide (DMPO) and 2,2,6,6-tetramethylpiperidine (TEMP) as a trapping agent. Furthermore, the degree of removal of organics in the final products for the different treatment methods is assessed by gas chromatography-mass spectrometer [GC–MS; GC: GC condition Agilent 7890B gas chromatograph and a column DB-5 (60 m × 0.25 mm × 0.25 μm), inlet temperature 230 °C, split ratio 10:1, injection volume 1 μL, helium (99.999%) as carrier gas (program: initial temperature: 40 °C, hold for 0 min, rise to 150 °C at 5 °C/min, hold for 10 min, rise to 300 °C at 20 °C/min, hold for 10 min); MS: MS condition Agilent 5977C, America, ionization mode Electron impact (EI), ionization energy 70 V volts, transfer line temperature 250 °C, ion source temperature 230 °C, quadrupole temperature 150 °C, scan range 10–550 *m/z*, solvent delay 8 min]. The samples are treated with HCl-butanol derivatization to ensure that all the organic acid groups are protonated, to ease subsequent separations. The chemical structure of various organic compounds in Bayer liquor is determined by computer spectral library search and manual analysis, and their percentage content is calculated by area normalization method.

3. Results and discussion

3.1. Properties of ultrasonic field

The cavitation threshold is the minimum sound intensity or sound pressure amplitude at which ultrasonic in the liquid medium produce cavitation. Cavitation is possible only when the sound intensity exceeds the cavitation threshold. The common method to quantitatively characterize the cavitation threshold is mainly iodine release method and UV–vis spectroscopy. Previous studies have shown that potassium iodide solution can be reduced to iodine after ultrasonic irradiation, as shown in Eqs. (4)–(6) [39]. If a small amount of carbon tetrachloride (CCl_4) is added to the solution, the output of iodine can be significantly increased, as shown in Eqs. (7)–(9). Iodine in solution can turn blue due to starch. Once sodium thiosulfate is added, the blue color disappears, as shown in Eq. (10). Therefore, the consumption of sodium thiosulfate solution can be used to indirectly measure the yield of acoustic cavitation.

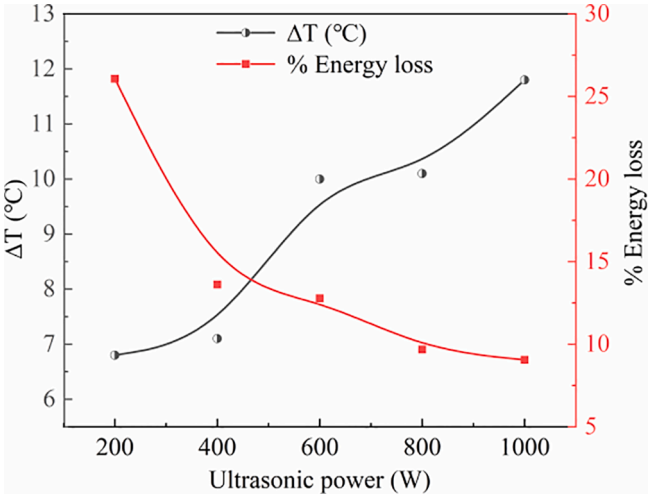

Fig. 3. % Energy loss of acoustic cavitation in Bayer liquor obtained by reaction calorimetry.

$$H_2O \xrightarrow{cavitation} H^{\cdot} + {}^{\cdot}OH \quad (4)$$

$$2\,{}^{\cdot}OH \rightarrow H_2O_2 \quad (5)$$

$$H_2O_2 + 2KI \rightarrow I_2 + 2KOH \quad (6)$$

$$CCl_4 + H_2O \rightarrow Cl_2 + CO + 2HCl \quad (7)$$

$$HCl + [O] \rightarrow Cl_2 + H_2O \quad (8)$$

$$2KI + Cl_2 \rightarrow 2KCl + I_2 \quad (9)$$

$$I_2 + \text{starch (blue)} \xrightarrow{2Na_2S_2O_3} 2NaI + Na_2S_4O_6\ (\textit{blue disapper}) \quad (10)$$

The relationship between ultrasonic power and iodine release is shown in Fig. 2(a). It can be seen that an increase in ultrasonic power increases iodine release with the maximum acoustic cavitation effect at 600 W.

The excess iodine ion in the solution react with iodine to form I_3^-, which has extremely high sensitivity at a wavelength of UV 354 nm (Eq. (11)) [40]. Based on this principle the yield of acoustic cavitation can be indirectly measured by ΔA_{354} (absorbance change at UV 354 nm) of I_3^-.

The relationship between ultrasonic power and ΔA_{354} of potassium iodide solution is shown in Fig. 2(b). It can be seen that an increase in ultrasonic power increases ΔA_{354} and the trend is in accordance with the I_2, with the maximum at 600 W.

$$I_2 + I^- \rightleftarrows I_3^- \quad (11)$$

The thermal effect of Bayer liquor on sonolysis can be measured using reaction calorimetry [41]. The temperature change (ΔT) of Bayer liquor during sonolysis is measured by a precise thermometer. The enthalpy change can be calculated, as shown in Eq. (12),

$$Q = C_p \times \Delta T \times m \quad (12)$$

where Q and C_p represent the heat and constant pressure heat capacity, respectively. The solution mass is represented by m. C_p of Bayer liquor is generally maintained at around 3.68 kJ/kg•℃. The % energy loss can be calculated, as shown in Eq. (13).

$$\%\ Energy\ loss = \frac{\Delta T \times C_p \times \rho}{t \times W} \times 100\% \quad (13)$$

where W represents the ultrasonic power, t represents the treatment time, and ρ represents the density of Bayer liquor. The % energy loss of acoustic cavitation in due to reaction calorimetry is shown in Fig. 3. It can be found that the % energy loss shows a decreasing trend with the increase of ultrasonic power. At an ultrasonic power of 600 W, the energy utilization is 87.22%.

3.2. Reaction kinetics

The kinetics of TOC removal in various systems are shown in Fig. 4 and Table 2. The results show that the combined US/O_3 system is more efficient as compared to standalone US and O_3 systems. A comparison of the three methods indicate a reduction in TOC concentrations of 6.79 g/L, 5.05 g/L and 3.16 g/L respectively, which correspond to a removal efficiency of 14.32%, 36.28% and 60.13%. In conclusion, the oxidation effect of US/O_3 system is far higher than the sum of the invidaul effects of single US and O_3.

In order to understand the mechanism of TOC removal, kinetic analysis is carried out under optimal conditions. The pseudo-first-order kinetic model and pseudo-second-order kinetic model for TOC removal in various systems are represented using Eq. (14) and (15), respectively [42,43].

$$\ln\left(\frac{TOC_0}{TOC}\right) = kt + b \quad (14)$$

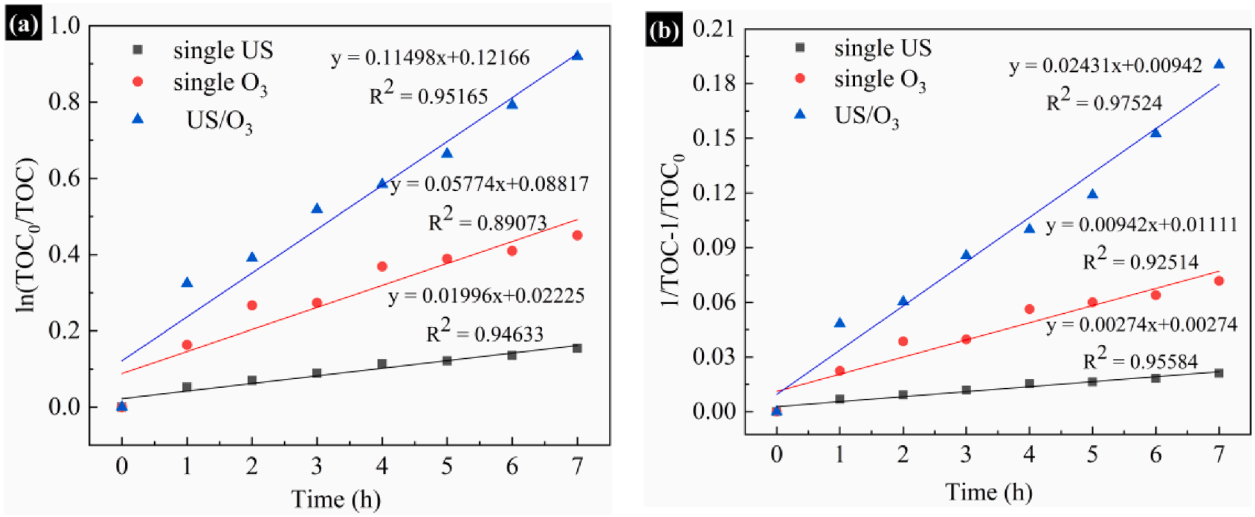

Fig. 4. Kinetics of TOC removal in various systems; (a) pseudo-first-order kinetic model; (b) pseudo-second-order kinetic model.

Table 2
Apparent rate constants and correlation coefficients of TOC removal in various systems.

Test	Ultrasonic power (W)	Ozone concentra-tion (g/h)	T (℃)	t (h)	Pseudo-first-order kinetic model		Pseudo-second-order kinetic model	
					k (1/h)	R^2	k (L/(g•h))	R^2
single US	600	/	55	7	1.996×10^{-2}	0.946	2.740×10^{-3}	0.959
single O_3	/	7.65	55	7	5.774×10^{-2}	0.891	9.420×10^{-3}	0.925
US/O_3	600	7.65	55	7	1.150×10^{-1}	0.952	2.431×10^{-2}	0.975

$$\frac{1}{\mathrm{TOC}} - \frac{1}{TOC_0} = kt + b \tag{15}$$

where TOC_0, TOC, and k are defined as initial TOC concentration, instantaneous TOC concentration and apparent rate constant, respectively. It can be observed for various systems the regression coefficients of the pseudo-first-order kinetic models ($R^2 = 0.891$–0.952) are less than that of the pseudo-second-order kinetic models ($R^2 = 0.925$–0.975). Therefore, the TOC removal process appears to follow a pseudo-second-order kinetic model, suggesting that the apparent rate constant may be proportional to the quadratic of species concentration. Table 2 shows the apparent rate constants and correlation coefficients of TOC removal of various systems, which clearly indicates that the combined treatment is far higher than the sum of rate constants of both the standalone treatment methods, confirming superiority of the synergic effect of the sonalysis and ozonation. Its magnitude can be described using enhancement factor (E), as shown in Eq. (16). $E > 1$, indicate synergistic effect; $E = 1$, indicate no synergistic effect; $E < 1$, indicate inhibitory effect.

$$\mathrm{E} = \frac{k_{US/O_3}}{k_{US} + k_{O_3}} \tag{16}$$

The results show E of 1.999 confirming the synergic effect. Ultrasonic promotes ozone to produce more •OH facilitating increased oxidation rate, thereby shorten reaction duration, ozone consumption and improve overall economics.

The advantage of combined US/O_3 process over standalone O_3 can be attributed to two aspects: (i) formation of excess •OH upon the thermal decomposition of O_3 and (ii) the reduction in the mass transfer resistance due to cavitation effect of US, facilitating higher transfer rate of O_3. Studies have shown that simultaneous introduction of O_3 and US results in additional pathway of •OH generation due to implosive collapse of O_3 [44]. When ultrasonic and ozone are combined, ozone is thermolysed in the cavitation bubbles, as shown in Eqs. (17) and (18) [38,45].

$$\mathrm{O_3} + US \rightarrow O_2 + O(^3P) \tag{17}$$

$$O(^3P) + H_2O \rightarrow 2\,^{\cdot}OH \tag{18}$$

The % removal of organic matter in US/O_3 system is effectively increased, since 1 mol ozone molecule decompose to 2 mol •OH, as against the generation of only 1 mol •OH for standalone O_3 system [3]. The type of reactions of •OH with organic compounds are: (i) extraction of hydrogen from C—H, N—H or O—H bond (Eq. (19)), (ii) radical–radical interactions (addition of molecular O_2, forming peroxy radicals) (Eq. (20)), and (iii) direct electron transfer producing oxidative intermediates (Eq. (21)). Finally, the organics are mineralized to inorganic salts, CO_2 and H_2O [46,47].

$$^{\cdot}OH + RH \rightarrow H_2O + R^{\cdot} \tag{19}$$

$$R^{\cdot} + O_2 \rightarrow RO_2^{\cdot} \tag{20}$$

$$^{\cdot}OH + RX \rightarrow RX^{\cdot+} + HO^- \tag{21}$$

The RH and RX represent the organic compounds, while their radicals are represented by $R^{\bullet}$, $RO_2^{\bullet}$ and $RX^{\bullet+}$. Differnt organic anions are formed as high molecular weight compounds are broken into low molecular weight compounds [48]. However, this improvement is subject to the following limitations: (i) the reactivity of molecular O_3 with organics and their oxidation by-products and (ii) the gas-phase decomposition of O_3 to more reactive radical species [28].

3.3. Effect of operating parameters

3.3.1. Effect of ozone concentration

The ozonation process contributes through direct ozonation and through indirect •OH oxidation based on solution pH. The ozone molecules can directly react with a few organic species in acidic media, while in alkaline media, ozone molecules mainly undergo indirect reactions by non-selective oxidation [49]. This can be attributed to the free radicals generated by the chain reaction of ozone molecules with any organic compounds. Eqs. (22) and (23) present radicals from ozone molecules; Eqs. (24)–(31) show a series of chain reactions and radicals formed during the ozonation process [3].

$$\mathrm{O_3} + OH^- \rightarrow HO_2^- + O_2 \tag{22}$$

$$\mathrm{O_3} + HO_2^- \rightarrow HO_2^{\cdot} + O_3^{\cdot-} \tag{23}$$

$$HO_2^{\cdot} \rightarrow O_2^{\cdot-} + H^+ \tag{24}$$

$$O_2^{\cdot-} + H^+ \rightarrow HO_2^{\cdot} \tag{25}$$

$$\mathrm{O_3} + O_2^{\cdot-} \rightarrow O_3^{\cdot-} + O_2 \tag{26}$$

$$O_3^{\cdot-} + H^+ \rightarrow HO_3^{\cdot} \tag{27}$$

$$HO_3^{\cdot} \rightarrow O_3^{\cdot-} + H^+ \tag{28}$$

$$HO_3^{\cdot} \rightarrow {}^{\cdot}OH + O_2 \tag{29}$$

$$\mathrm{O_3} + {}^{\cdot}OH \rightarrow HO_4^{\cdot} \tag{30}$$

$$HO_4^{\cdot} \rightarrow HO_2^{\cdot} + O_2 \tag{31}$$

The effect of ozone on decomposition of organics from strongly alkaline Bayer liquor is evaluated for a duration of 1 h to 7 h, at a temperature of 55 °C, covering ozone concentration of 2.68 to 7.65 g/h and the results are presented in Fig. 5(a)–(c). With the increase of ozone concentration, the residual TOC concentration decreased from 6.39 to 5.05 g/L, and the TOC % removal increased significantly from 19.37 to 37.16%. Furthermore, at ozone concentration of 2.68 and 5.24 g/h, the concentration of oxalate decreased marginally after 7 h of oxidation. A decomposition in the range of 18.25 to 20.44% could be achieved, due to resistant macro organic molecules oxidized to oxalate. However, the concentration of oxalate increased significantly from 1.37 to 2.98 g/L at a ozone concentration of 7.65 g/h, due to decomposition of macromolecular organic matter oxidized as oxalate in large quantities. And at 7.65 g/h of ozone concentration, a 62% decolorization could be achieved after 1 h of oxidation. However, at 2.68 and 5.24 g/h of ozone concentration, the % decolorization is <22.6%. Based on the above experimental results, the optimal ozone concentration is selected as 7.65 g/h.

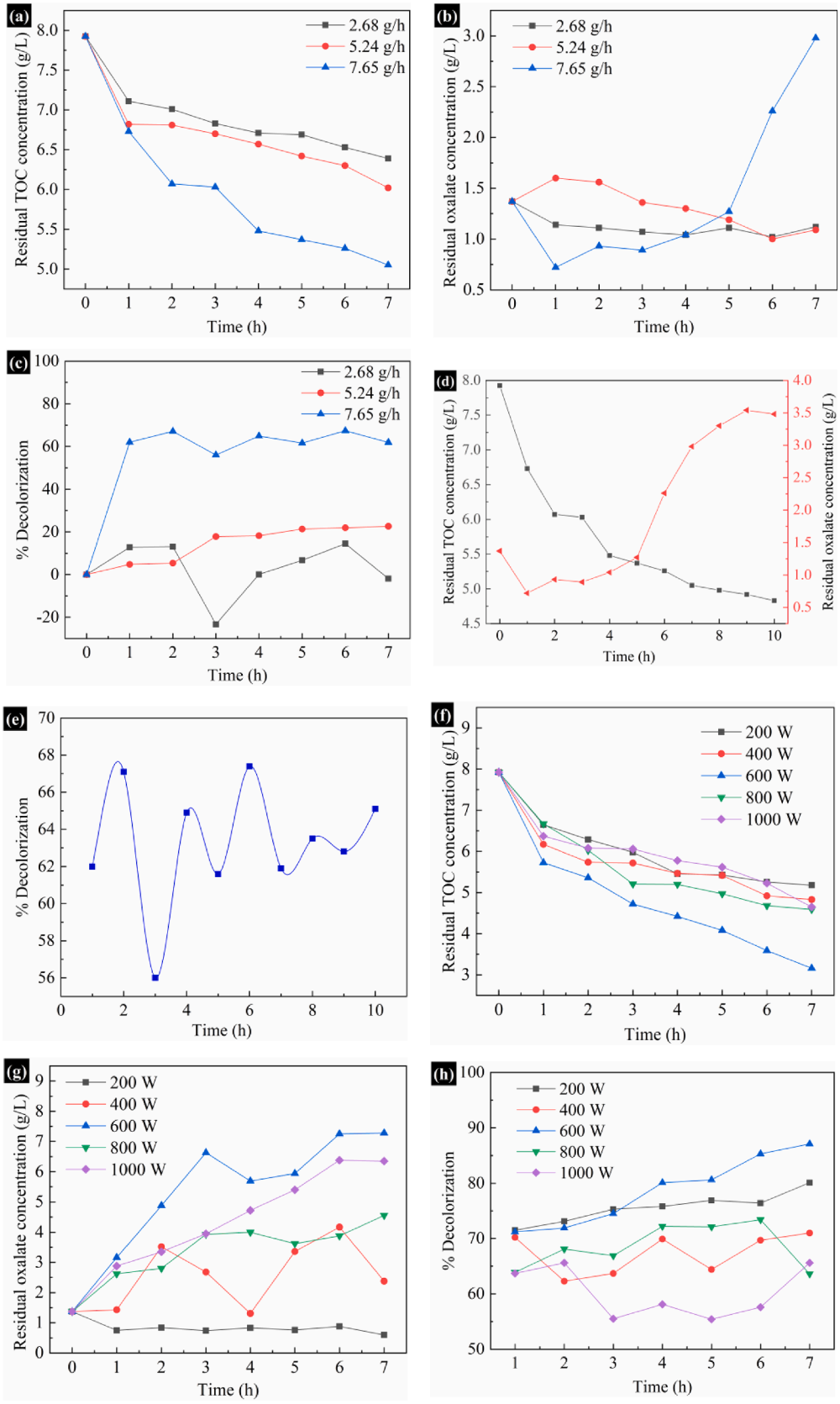

Fig. 5. (a) effect of ozone concentration on TOC removal; (b) effect of ozone concentration on oxalate removal; (c) effect of ozone concentration on the % decolorization; (d) effect of reaction duration on TOC removal and oxalate removal; (e) effect of reaction duration on the % decolorization; (f) effect of ultrasonic power on TOC removal; (g) effect of ultrasonic power on oxalate removal; (h) effect of ultrasonic power on the % decolorization. Conditions: (a)–(c): Bayer liquor 500 mL, reaction duration 7 h, ultrasonic power 600 W, temperature 55 °C, pH 14.4; (d)-(e): Bayer liquor 500 mL, ozone concentration 7.65 g/h, ultrasonic power 600 W, temperature 55 °C, pH 14.4; (f)-(h): Bayer liquor 500 mL, reaction duration 7 h, ozone concentration 7.65 g/h, temperature 55 °C, pH 14.4.

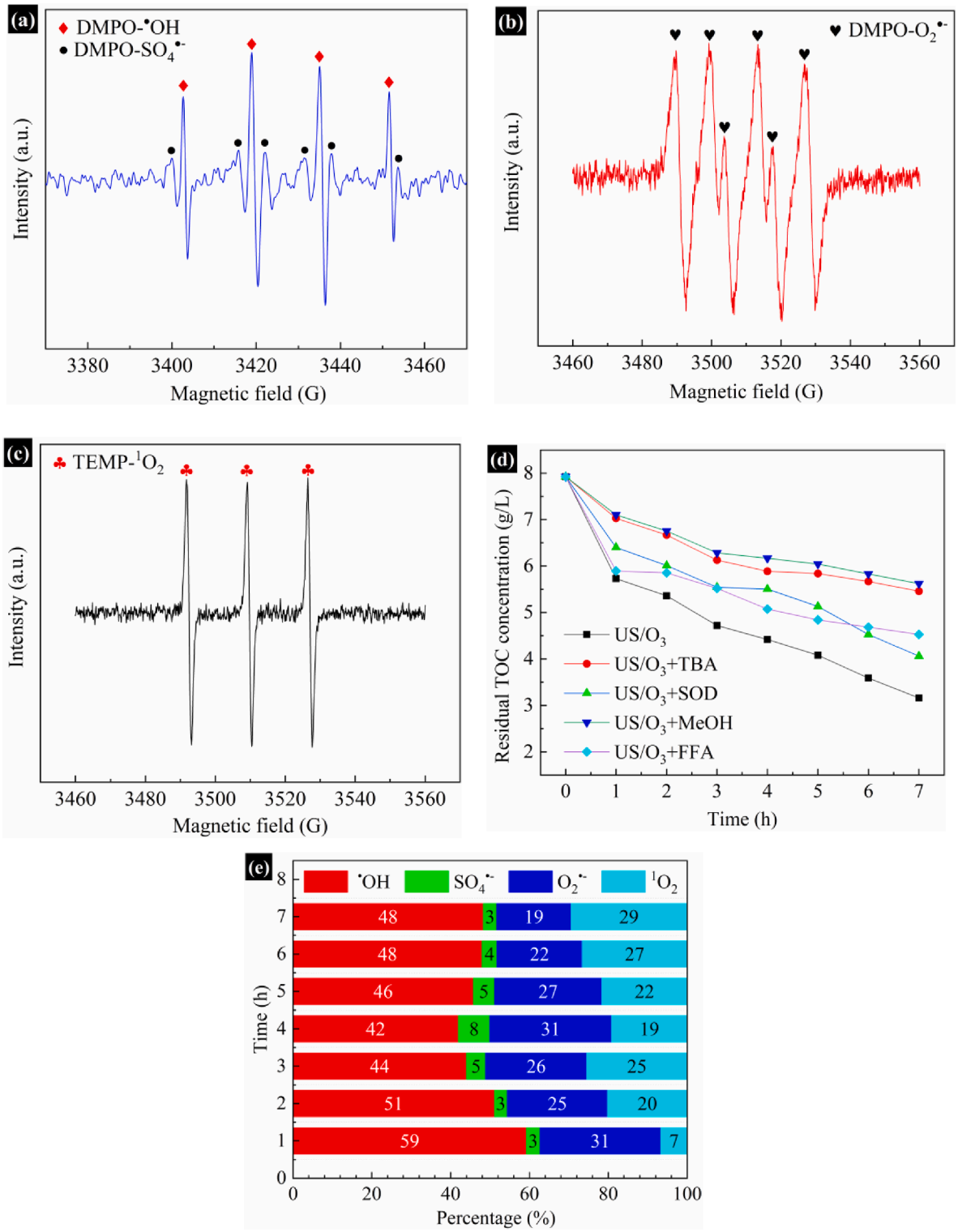

Fig. 6. Free radicals in Bayer liquor treated with US/O_3; (a) EPR spectra of $^{\bullet}OH$ and $SO_4^{\bullet-}$; (b) EPR spectra of $O_2^{\bullet-}$; (c) EPR spectra of $^1O_2$; (d) quenching effects; (e) Percentage of different ROS in the removal of TOC. Conditions: TBA 7.5 mol/L, SOD 500 mg/L, MeOH 8 mol/L, FFA 3 mol/L, Bayer liquor 500 mL, reaction duration 7 h, ozone concentration 7.65 g/h, ultrasonic power 600 W, temperature 55 °C, pH 14.4.

3.3.2. *Effects of reaction duration*

The effect of reaction duration on the decompostion of organics is assessed at a ozone concentration of 7.65 g/h, temperature of 55 °C, covering reaction duration of 1–10 h and the results are presented in Fig. 5(d) and (e). After 7 h of oxidation treatment, the concentration of TOC decreased from 7.925 to 5.05 g/L, a 37.16% reduction. When the reaction duration is increase to 10 h, the concentration of TOC decreased margianally with the total decomposition having increased only to 39.05%. However, the concentration of oxalate increased from 1.37 to 3.48 g/L, due to decomposition and accumulation of macromolecular organic matter as oxalate in large quantities. And the % decolorization is 62% after 1 h of oxidation, confirming significant decolorization due to

ozone oxidation. Any further increase in the reaction duration is insignificant for decolorization. Hence the optimal reaction duration is chosen as 7 h.

3.3.3. Effect of ultrasonic power

The main ways of removing organic pollutants by sonolysis are thermal decomposition inside cavitation bubbles and attack of •OH in solution, which will eventually lead to the formation of hydroxylated products [50]. The former mechanism is the main removal path for non-volatile compounds, while the second mechanism is usually predominant for volatile pollutants [51]. Moreover, the hot spot hypothesis suggests that the ultrasonic removal reaction may occur in three areas: (i) inside the cavitation bubbles, (ii) the interfacial region between cavitation bubbles and the bulk solution, and (iii) the bulk solution [52]. The •OH generated by aqueous solution sonolysis may either react in the gas phase or recombine at the cooler gas–liquid interface or in the solution bulk to produce hydrogen peroxide and water, as shown in Eqs. (32)–(35) [53]:

$$H_2O \rightarrow {}^{\cdot}OH + {}^{\cdot}H \ (thermal \text{ decomposition}) \quad (32)$$

$${}^{\cdot}OH + {}^{\cdot}H \rightarrow H_2O \quad (33)$$

$$2\,{}^{\cdot}OH \rightarrow H_2O_2 \quad (34)$$

$$2\,{}^{\cdot}H \rightarrow H_2 \quad (35)$$

If the solution is saturated with oxygen, peroxyl and more •OH radicals are formed in the cavitation bubble itself, and additional H_2O_2 is produced at the gas–liquid interface or in the solution bulk, as shown in Eqs. (36)–(39):

$$O_2^{\cdot} + {}^{\cdot}H \rightarrow HO_2^{\cdot} \quad (36)$$

$$O_2 \rightarrow O + O \quad (37)$$

$$O + H_2O \rightarrow {}^{\cdot}OH + {}^{\cdot}OH \quad (38)$$

$$HO_2^{\cdot} + HO_2^{\cdot} \rightarrow H_2O_2 + O_2 \quad (39)$$

The effect of ultrasonic on the removal of organics from strongly alkaline Bayer liquor is assessd for a reaction duration of 1 to 7 h, temperature of 55 °C, ozone concentration of 7.65 g/h, and ultrasonic power covering 200 to 1000 W. The results are compiled in Fig. 5(f)-(h). With an increase of ultrasonic power, the TOC is found to decrease until an ultrasonic power of 600 W, while it is found to decrease with further increase. At 600 W ultrasonic power, at duration of 7 h the residual TOC concentration decreased to 3.16 g/L, which correspond to % removal of 60.13%. On the other hand, the % decolorization is 71.2% within 1 h, which increased to 87.1% after 7 h. An increase in ultrasonic power is known to generate cavitation bubbles at higher temperatures that would cause acoustic screens and insufficient collapse of cavitation bubbles. In which case, more ozone molecules will be degassed and the proportion of •OH will decrease. This is consistent with the basic properties of ultrasonic (Section 3.1). Based on experimental results the optimal ultrasonic power is identified to be 600 W.

In conclusion, the following experimental conditions are identified to maximize the removal of organic matter in Bayer liquor: reaction duration; 7 h, ozone concentration; 7.65 g/h, ultrasonic power; 600 W, and temperature; 55 °C.

3.4. Evaluation of removal effect

3.4.1. Free radicals type analysis

Spin-trapping EPR is increasingly used to detect free radicals, in which 5,5-dimethyl-1-pyrroline *N*-oxide (DMPO) and 2,2,6,6-tetramethylpiperidine (TEMP) are commonly used as spin traps. •OH, $SO_4^{\bullet-}$ and $O_2^{\bullet-}$ can react with DMPO to form stable DMPO-•OH, DMPO-$SO_4^{\bullet-}$ and DMPO-$O_2^{\bullet-}$ adducts, respectively. $^1O_2$ can react with TEMP to form stable TEMP-$^1O_2$ adducts. The hyperfine splitting peaks of DMPO-$SO_4^{\bullet-}$ adducts generally have the following characteristics: 1:1:1:1:1:1 sextet, and their hyperfine splitting constants are $\alpha_N = 13.51$ G, $\alpha_{\beta\text{-H}} = 9.93$ G, $\alpha_{\gamma\text{-H1}} = 1.34$ G, $\alpha_{\gamma\text{-H2}} = 0.88$ G; the hyperfine splitting peaks of DMPO-•OH adducts generally have the following characteristics: 1:2:2:1, and their hyperfine splitting constants are $\alpha_N = 14.9$ G, $\alpha_{\beta\text{-H}} = 14.9$ G; the hyperfine splitting constants of DMPO-$O_2^{\bullet-}$ are $\alpha_N = 14.3$ G, $\alpha_{\beta\text{-H}} = 11.2$ G, $\alpha_{\gamma\text{-H1}} = 1.3$ G; the hyperfine splitting constants of TEMP-$^1O_2$ are $\alpha_N = 16.3$ G [54]. The EPR spectra of DMPO and TEMP-trapped radical adducts of Bayer liquor treated with US/O_3 are shown in Fig. 6(a)-(c). The results show that the types of free radicals are •OH, $SO_4^{\bullet-}$, $O_2^{\bullet-}$ and $^1O_2$. The Bayer liquor contains about 1.37 g/L SO_4^{2-}, so the possible source of $SO_4^{\bullet-}$ is shown in Eqs. (40) and (41) [55,56].

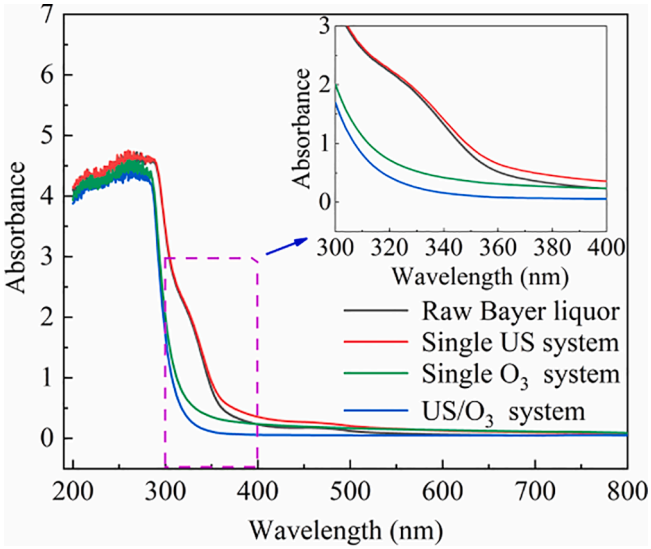

Fig. 7. UV–Vis absorbance spectrums of raw Bayer liquor and the sample subjected to 7 h oxidation in single US, single O_3 and US/O_3 systems.

$$H^+ + SO_4^{2-} \rightarrow HSO_4^- \quad (40)$$

$$HSO_4^- + {}^{\cdot}OH \rightarrow SO_4^{\bullet-} + H_2O \quad (41)$$

In addition, the contribution of different reactive oxygen species (ROS) in the removal of TOC is examined by quenching test. As we all known, *tert*-butanol (TBA), furfuryl alcohol (FFA) and superoxide dismutase (SOD) can be used as scavengers for •OH, $O_2^{\bullet-}$ and $^1O_2$. The difference in quenching between ethanol (EtOH) and TBA is used to examine the contribution of •OH and $SO_4^{\bullet-}$. The quenching test of different scavengers in removal of organics by US/O_3 are shown in Fig. 6 (d) and (e). The results show that the different scavengers significantly delayed the removal of organics, and the order of the oxidation effect is US + O_3 > US + O_3 + FFA > US + O_3 + SOD > US + O_3 + TBA > US + O_3 + MeOH. As a result, the order of the effects of various ROS in the removal of TOC is •OH > $O_2^{\bullet-}$ > $^1O_2$ > $SO_4^{\bullet-}$ after a duration of 1 h. The effects of different ROS changed significantly as the reaction duration is prolonged. The order of the effects of different ROS in the removal of TOC is •OH > $^1O_2$ > $O_2^{\bullet-}$ > $SO_4^{\bullet-}$, when the duration is 7 h.

3.4.2. UV–Vis analysis

UV–Vis is an electronic spectrum, mainly based on the molecular absorption of certain compounds in 200–800 nm spectral region. The band width of 200–400 nm is ultraviolet region while 400–800 nm is visible light region. Differene in UV–Vis absorption spectra represent valence electron. As stated by Yan et al., the chemical changes during the oxidation of dissolved organic matter (DOM) can be roughly compared using UV–Vis [57]. The effect of oxidation of organics can be

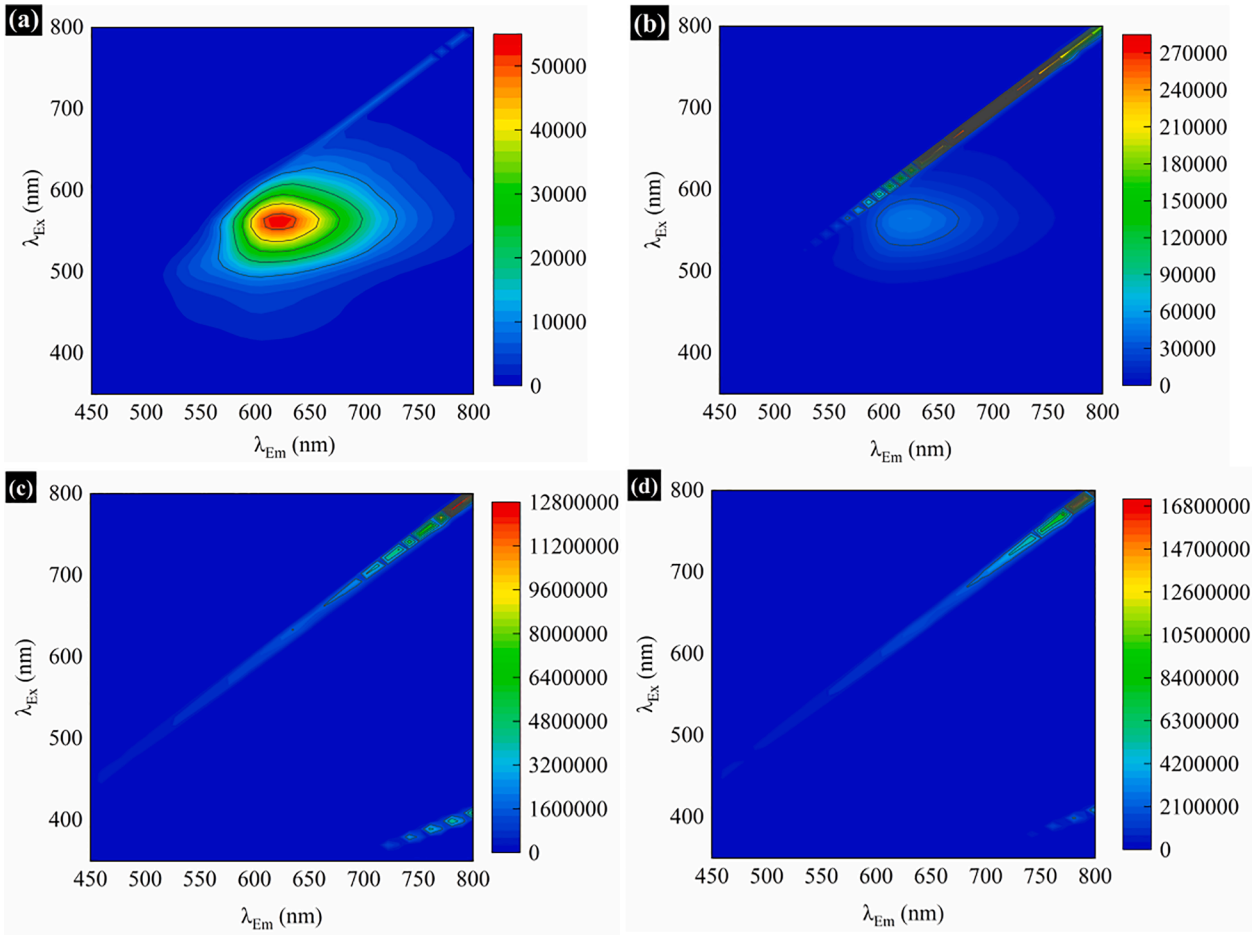

Fig. 8. Comparison of EEMS of Bayer liquor before and after oxidation for 7 h by the three different systems; (a) raw Bayer liquor, (b) in US system, (c) in O_3 system, (d) in US/O_3 system.

judged, which plays an important role in analyzing the types of chromophores. The UV–Vis absorbance spectrums of raw Bayer liquor and the sample subjected to 7 h oxidation with US, with O_3 and combination of US/O_3 systems are shown in Fig. 7.

The absorbance of samples oxidized by O_3 and US/O_3 for 7 h at 300–400 nm is obviously lower than the raw Bayer liquor, with a clear downward shift, indicating a reduction in organic matter concentration [58]. This phenomenon can be attributed to the decrease in the molar absorptivity of solution after oxidation, due to hypochromic effect. However, the absorption spectrum did not decrease after 7 h, indicating that US is not effective in the color reduction.

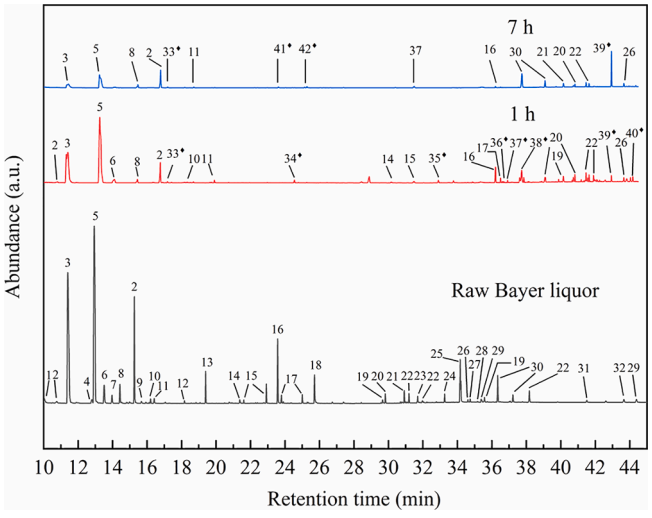

Fig. 9. Total-ion chromatogram of GC–MS for raw Bayer liquor and samples obtained after 1 h and 7 h of US/O_3 treatment (marked as by-products).

3.4.3. EEMS analysis

The relationship between the fluorescence intensity of a substance and the change of excitation wavelength and emission wavelength is assessed using excitation emission matrix spectroscopy (EEMS). Ever since EEMS is used by American marine chemist Coble et al. to study the fluorescence properties of dissolved organic matter (DOM) in the Black Sea, it is widely being utilized to characterize type and source of DOM in water [59]. Furthermore, EEMS has been shown to be a particularly effective to study the complexation of metal ions with humic materials. The comparison of EEMS of Bayer liquor before and after oxidation for 7 h by the three different systems are shown in Fig. 8. It can be clearly seen that there are two scattering peaks, belonging to first-order Rayleigh scattering (distributed along $\lambda_{Em} = \lambda_{Ex}$) and Raman scattering, respectively.

The raw Bayer liquor (Fig. 8(a)) has a single and complete characteristic peak ($\lambda_{Em}/\lambda_{Ex}$: 625 nm/550 nm), and the spectral lines are densely distributed, indicating high purity, mainly due to polycyclic aromatic hydrocarbons with complex structure and high content of fluorescent components. Contrary to the results of Elkins et al. [60], this study found the characteristic peaks of humic organic compounds having significant red shift (i.e. moved to the long-wave direction), indicating the conjugation effect of large molecular compounds with

Table 3
Organic components in raw Bayer liquor and after treatment with US/O_3 for 1 h and 7 h.

No.	Compounds	Structure formula	Confidence (%)	Relative content (%)		
				Raw Bayer liquor	1 h	7 h
1	(s)-2-methyl-1-butanol	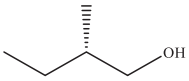	92.4	0.66	/	/
2	butanoic acid	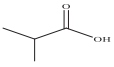	92.3	8.19	6.98	17.83
3	acetic acid		97.9	26.54	34.9	9.71
4	4-heptanone	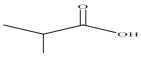	97.4	0.56	/	/
5	*n*-butyl ether		97	32.36	30.15	30.12
6	propanoic acid	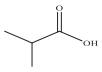	98	2.26	2.76	/
7	3-methyl-4-heptanone	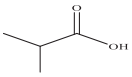	98	0.78	/	/
8	2-methyl-propanoic acid		98.2	1.56	1.48	2.9
9	3-pentyl-carbonic acid	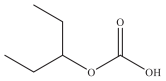	72.9	0.23	/	/
10	3-methyl-butanoic acid	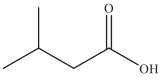	97.1	0.3	0.23	/
11	dibutoxymethane		89.9	0.43	0.36	0.43
12	di-*tert*-butyl ether	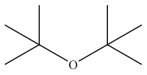	82.9	0.19	/	/
13	1-butoxy-1-isobutoxy-butane	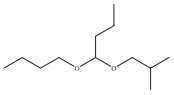	97	1.85	/	/
14	benzoic acid	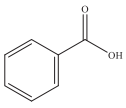	94.6	0.32	0.39	/
15	formic acid	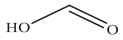	78.9	1.4	0.78	/
16	butanedioic acid	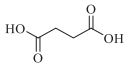	96.7	4.39	4.3	0.64
17	glutaric acid	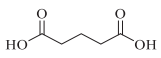	91.6	1.22	1.76	/
18	4-hydroxy-benzoic acid	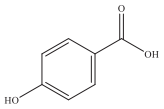	96.5	2.66	/	/
19	4-trimellitsaeureanhydrid	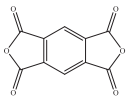	87.4	0.75	1.14	/
20	1,2-benzenedicarboxylic acid	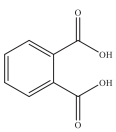	88.3	0.62	1.84	1.2
21	1,3-benzenedicarboxylic acid	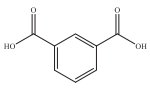	94.1	0.72	/	2.5

(*continued on next page*)

Table 3 (*continued*)

No.	Compounds	Structure formula	Confidence (%)	Relative content (%)		
				Raw Bayer liquor	1 h	7 h
22	1,4-benzenedicarboxylic acid	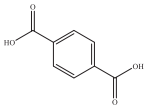	94.3	0.73	3.49	2.98
23	phenylphosphonic acid	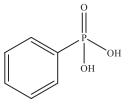	57.8	0.52	/	/
24	tris(2-ethylhexyl)amine	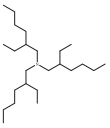	93.2	0.58	/	/
25	5-hydroxy-1,3-benzenedicarboxylic acid	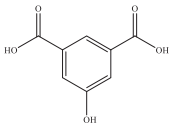	69	3.1	/	/
26	hexanedioic acid	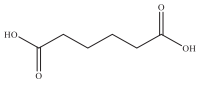	94.4	1.52	1.97	1.46
27	2,5-dichlorophenyl isophthalic acid	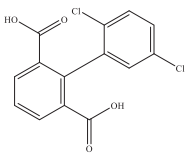	48.2	0.19	/	/
28	3-benzyl-2-*t*-butyl-4-oxoimidazolidine-1-carboxylic acid	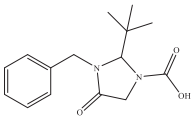	65.5	0.25	/	/
29	3-(((3-methylbutan-2-yl)oxy)carbonyl)benzoic acid	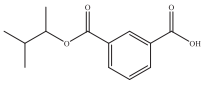	54.2	0.8	/	/
30	1,2,4-benzenetricarboxylic acid	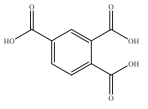	87.4	2.67	/	7.74
31	2-amino-5-iodobenzoic acid	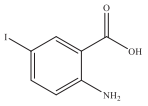	54.1	0.24	/	/
32	3,4-bis(*tert*-butylsulfanyl)-1-phenylpyrrole-2,5-dione	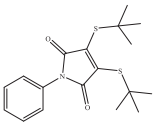	52.3	0.4	/	/
33	2,4-dimethyl-3-pentanol	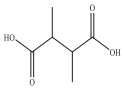	88.9	/	0.31	0.64
34	1,1-dibutoxy-butane	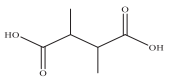	87.7	/	0.55	/
35	propanedioic acid	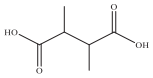	91.6	/	0.3	/
36	2,3-dimethyl-butanedioic acid	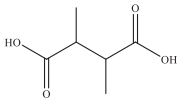	89.5	/	0.23	/
37	1,1,3,3-tetrabutoxy-2-propanone	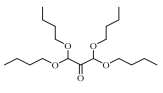	71.5	/	0.22	1.55

(*continued on next page*)

Table 3 (*continued*)

No.	Compounds	Structure formula	Confidence (%)	Relative content (%)		
				Raw Bayer liquor	1 h	7 h
38	*n*-propyl-2-hydroxy-1-oxohexahydro-1 h-azepine	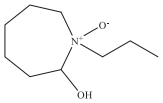	88.9	/	0.3	/
39	n,*n*-dioctyl-1-octanamine	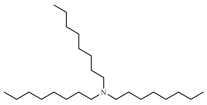	91.3	/	0.64	17.33
40	1,2-ethanediylbis[bis(1-methylethyl)-phosphine	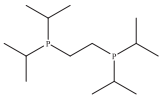	53.2	/	0.91	/
41	2,3-dimethyl-2-pentenoic acid	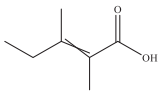	79.1	/	/	0.59
42	3-methyl-3-nonanol	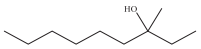	74.8	/	/	0.97

aromatic structures. These compounds form dimers or multimers at higher concentrations, resulting in the transfer of energy back and forth between the component molecules, extending the life of the molecules before being irradiated by fluorescence. Ultrasonic treatment can change the physicochemical properties of the solution, which may lead to depolymerization of some macromolecular compounds in the aggregated state, resulting in the exfoliation of luminescent groups and the formation of non-aggregated long-chain carbons. However, it is easy to be bent resulting in a significant decrease in fluorescence efficiency, thus showing the phenomenon of sparse spectrum, as shown in Fig. 8(b). The Bayer liquor treated with O_3 and US/O_3, the characteristic peaks are hardly seen, except first-order Rayleigh scattering and Raman scattering, as shown in Fig. 8 (c) and (d). The possible explanation could be that most of the aggregated high molecular compounds are oxidized and removed by $^{\bullet}$OH, forming short-chain carbons and some long-chain carbons with very low concentrations, resulting in a significant decrease in fluorescence intensity.

3.4.4. GC–MS analysis

The total-ion chromatogram of GC–MS of raw Bayer liquor and samples after 1 h and 7 h of US/O_3 treatment are shown in Fig. 9. Comparing the characteristic ions (Fig. 9) with the data in the spectral library, the organic components in raw Bayer liquor and samples treated with US/O_3 for 1 h and 7 h are deduced, as shown in Table 3. The HCl-butanol derivatization confirms presence of large amount of *n*-butyl ether (25.12–43.46%) could be attributed to condensation of two equivalents of *n*-butanol during butyl esterification process. Table 3 presents, 31 types of organic compounds exist in raw bayer liquor which include 23 organic acids, 3 ketones, 2 alkanes, 1 amine, 1 alcohol and 1 ether. specifically, the 23 organic acids include butanoic acid, acetic acid, propanoic acid, 2-methyl-propanoic acid, 3-pentyl-carbonic acid, 3-methyl-butanoic acid, benzoic acid, formic acid, butanedioic acid, glutaric acid, 4-hydroxy-benzoic acid, 4-trimellitsaeureanhydrid, 1,2-benzenedicarboxylic acid, 1,3-benzenedicarboxylic acid, 1,4-benzenedicarboxylic acid, phenylphosphonic acid, 5-hydroxy-1,3-benzenedicarboxylic acid, hexanedioic acid, 2,5-dichlorophenyl isophthalic acid, 3-benzyl-2-*t*-butyl-4-oxoimidazolidine-1-carboxylic acid, 3-(((3-methylbutan-2-yl)oxy)carbonyl)benzoic acid, 1,2,4-benzenetricarboxylic acid and 2-amino-5-iodobenzoic acid; 3 ketones include 4-heptanone, 3,4-bis (*tert*-butylsulfanyl)-1-phenylpyrrole-2,5-dione and 3-methyl-4-heptanone; 2 alkanes include dibutoxymethane and 1-butoxy-1-isobutoxybutane; 1 amine include tris(2-ethylhexyl)amine; 1 alcohol include (*s*)-2-methyl-1-butanol; 1 ether include di-*tert*-butyl ether. Furthermore, the characteristic peaks of Bayer liquor are significantly reduced after being treated with US/O_3 for 1 h, which could be attributed to the significant reduction in the chromophores. These chromophores mainly include some aromatic compounds and other unsaturated cmpounds such as polyphenols, quinones, C═O and C═C. After US/O_3 treatment for 7 h, the organic compounds are significantly oxidized, and only 10 species remained, mainly including aldehydes, amines, alkanes, alcohols and some organic acids, while other are transformed or completely mineralized.

3.5. Removal mechanism

The humate molecules in bauxite is degraded in the Bayer process to form many organic compounds, which contain single benzene rings, other unsaturated bonds and various simple substituents, mainly carboxylic acids and some hydroxyl groups. Various aliphatic compounds are formed by degrading the substituents that are cleaved from the benzene rings in the original humate molecule. According to reports, the removal of organics in the US/O_3 system is generally through reactions mediated by $^{\bullet}$OH, ozone, hydrogen peroxide, and pyrolysis [61]. This process can increase the degree and rate of removal of organic matter, due to the decomposition of aromatic compounds and other unsaturated bonds. The opening of benzene ring has been considered to be a strong evidence for the conversion of aromatic to aliphatic compounds. As the degree of benzene ring breakage continues to increase, it polymerizes to form larger aliphatic compounds.

Fig. 10 shows the general reaction pathways for the removal of typical organics in Bayer liquor by US/O_3. It can be seen from Table 3 that the unsaturated organic compounds such as 4-hydroxy-benzoic acid and 5-hydroxy-1,3-benzenedicarboxylic acid, are not only high but can be thoroughly removed and hence these two organic compounds are selected as typical representatives. The electrophilic addition reaction of $^{\bullet}$OH to aromatic rings is the main factor that constitutes the reaction mechanism of $^{\bullet}$OH and aromatic compounds [62].

The 4-hydroxy-benzoic acid is oxidized and removed by $^{\bullet}$OH, through either of the two paths. (i) Decarboxylation reaction: $^{\bullet}$OH cleave C—C bond connecting the benzene ring and the carboxylic acid, and the carboxyl group is removed to generate hydroquinone. $^{\bullet}$OH continue to oxidize phenolic products to generate peroxyl peroxy radicals in the benzene ring, which lead to cleavage of the benzene ring through dimerization to generate maleic acid and fumaric acid. (ii) Dehydrogenation substitution reaction: the hydroxyl groups (–OH) on 4-hydroxy-benzoic acid belongs to the activating group, which can promote the substitution reaction of the hydrogen atom on its vicinal position. Therefore, $^{\bullet}$OH preferentially attacks the vicinal position of the

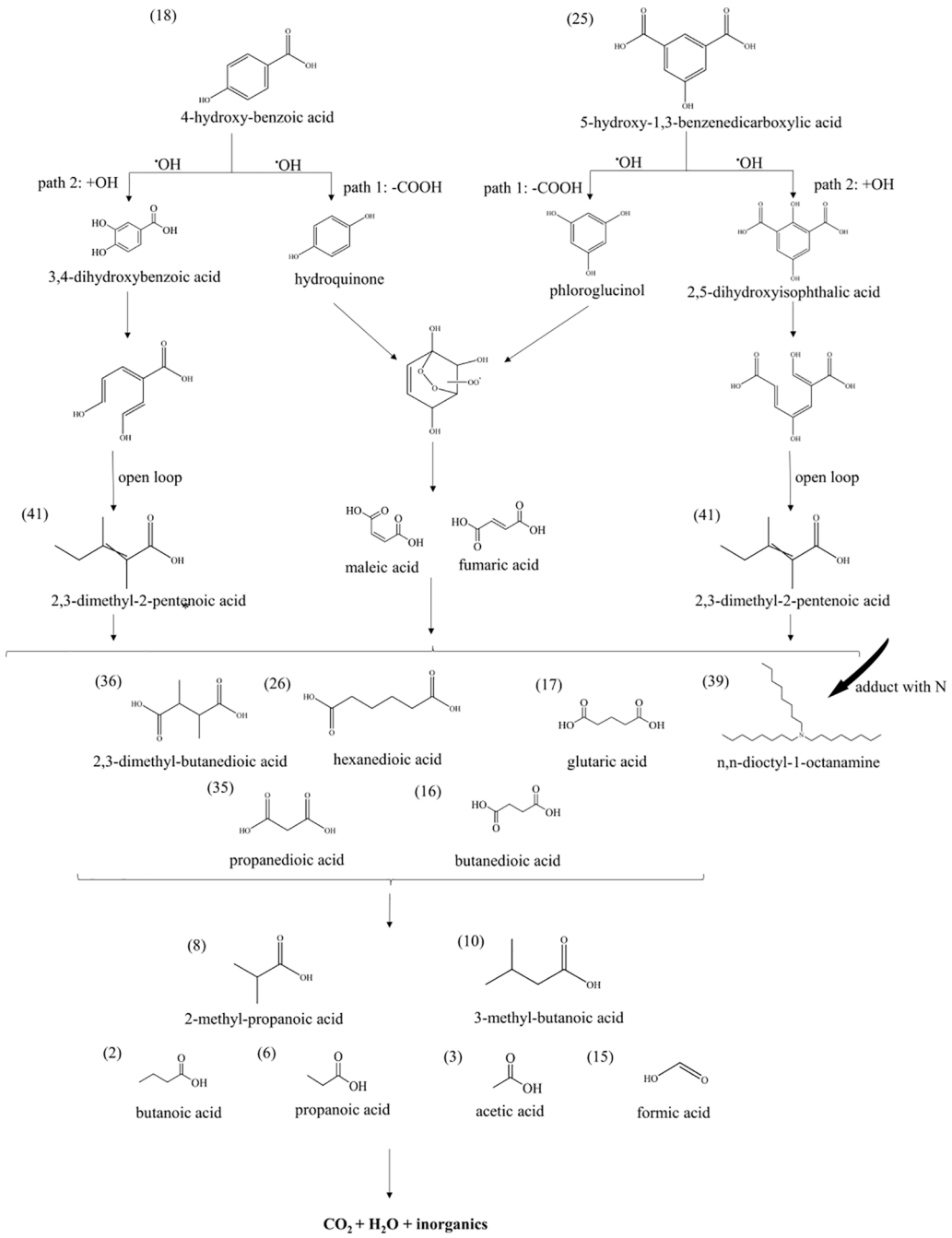

Fig. 10. General reaction pathways for the removal of typical organics in Bayer liquor by US/O_3.

aromatic ring of –OH functional group, and then the substitution reaction of hydrogen extraction occurs to generate the hydroxylated product 3,4-dihydroxybenzoic acid. •OH continue to attack the H atom at the ortho position of the carboxyl group on 3,4-dihydroxy-benzoic acid, and a hydrogen extraction substitution reaction occurs, and then C═C bond containing two –OH is cleaved, and the benzene ring is cracked to generate 2,3-dimethyl-2-pentenoic acid. The oxidation process of 5-hydroxy-1,3-benzenedicarboxylic acid is similar to that of 4-hydroxy-benzoic acid. On the one hand, it can form phloroglucinol through decarboxylation reaction, and then form peroxy radicals in the benzene ring; on the other hand, it can also form 2,5-dihydroxyisophthalic acid through dehydrogenation substitution reaction, and the continuous attack of •OH radical leads to cleavage of the benzene ring to form 2,3-dimethyl-2-pentenoic acid. •OH radical reacts with C═C bond of the butenedioic acid and 2,3-dimethyl-2-pentenoic acid to form 2,3-dimethyl-butanedioic acid, hexanedioic acid, glutaric acid, propanedioic acid, butanedioic acid and n,*n*-dioctyl-1-octanamine (adduct with N). Then, the above products are continuously oxidized by •OH radical, cutting off the C—C bond at the terminal carbon position, and gradually removing the carboxyl group to generate 4C, 3C and 2C products (i.e. 2-methyl-propanoic acid, 3-methyl-butanoic acid, butanoic acid, propanoic acid, acetic acid, formic acid), which can finally be mineralized to generate CO_2, H_2O and inorganics. In addition, the above mechanism is also applicable to the oxidative degradation process of other polycarboxylic acids.

3.6. Economic evaluation

The cost of removing TOC consists of total capital cost and operating and maintaining (O&M), where the cost involved in O&M system

includes part replacement cost, chemical cost, and electrical cost [63]. Assuming the total capital cost is P, the annual replacement cost of ultrasonic and ozone equipment parts is about 0.02P, and analytical cost is 0.1P-0.3P. Since products such as catalysts are not added, the chemical price is 0. Ozone is often produced onsite due to its chemical instability, with the most common equipment using corona discharge systems. The energy demand of such an ozone generator can vary between 8 and 20 kWh/kg_{O3}. The energy density of ultrasound in this experiment is 1.2 W/mL, which results in very high equipment capital costs and higher O&M costs. Therefore, there is an urgent need to use the lowest possible energy density to make the process more feasible, which can be achieved by using larger throughputs. The premise that the US/O_3 process is economically feasible on an industrial scale is that its energy density should not exceed 0.05 W/mL. Therefore, we roughly measure the economic benefits of this process through the cost of ozone. For every 1 ton of TOC processed, the ozone consumption is 3.49–11.24 ton, with an average of 8.16 ton. Electricity is calculated at a rate of $0.08/kWh. Therefore, the average consumption of this process for 1 ton of TOC is 5,222 USD, and the minimum consumption is 2,233 USD. The average price of 1 ton of TOC processed in the industry is 5,000 USD at present. In summary, the US/O_3 process for the removal of organic matter from Bayer liquor has considerable feasibility in the industrial field.

4. Conclusions

This work harnessed UV–vis analysis, EEMS analysis and GC–MS analysis to understand the underlying mechanisms for the removal of organic matter from Bayer liquor utilizing combined US/O_3 process. The following are the major conclusions and are summarized below:

(1) The effect of operating parameters such as reaction duration, ozone concentration, and ultrasonic power are found to influence degradation of organics using the combined US/O_3 process. The TOC concentration decreased from 7.925 to 3.16 g/L with a duration of 7 h, at a ozone concentration of 7.65 g/h and at a ultrasonic power of 600 W, along with the % decolorization of 87.1%.
(2) The removal of organic matter followed the pseudo-second-order reaction kinetics, and the calculated apparent rate constant (k) for US, O_3 and combined US/O_3 systems to be 2.74×10^{-3} L/(g•h), 9.42×10^{-3} L/(g•h) and 2.431×10^{-2} L/(g•h), indicating the synergistic effect to be significantly dominant as compared to the standalone systems.
(3) The order of the effects of different ROS in the removal of TOC is $^{\bullet}OH > {}^1O_2 > O_2^{\bullet-} > SO_4^{\bullet-}$, when the duration is 7 h.
(4) Of the 31 different types of organics detected in the Bayer liquor, 21 are transformed or completely mineralized by the combined US/O_3 treatment. The possible removal mechanism is identified which include decarboxylation reaction, dehydrogenation substitution reaction and the cleavage of the benzene ring.

The results highlight the potential of synergic/combined effect of US/O_3 treatment system to serve as a viable process that could alter the existing waste water handling sytems of alumina production process.

CRediT authorship contribution statement

Jianfeng Ran: Methodology, Investigation, Writing – original draft. **Haisheng Duan:** Resources. **C. Srinivasakannan:** Formal analysis. **Jiashu Yao:** Data curation. **Shaohua Yin:** Funding acquisition, Conceptualization, Supervision, Writing – review & editing. **Libo Zhang:** Project administration, Writing – review & editing.

Declaration of Competing Interest

The authors declare that they have no known competing financial interests or personal relationships that could have appeared to influence the work reported in this paper.

Acknowledgments

Funding: This work was supported by Yunnan Major Scientific and Technological Projects (grant NO. 202202AG050011) and Yunnan Ten Thousand Talents Plan Young & Elite Talents Project (grant NO. YNWR-QNBJ-2018-323).

References

[1] Y. Zhang, R. Xu, H. Tang, L. Wang, W. Sun, A review on approaches for hazardous organics removal from Bayer liquors, J. Hazard. Mater. 397 (2020), 122772.
[2] M.A. Soplin, A.B.B. Junior, M.P.G. Baltazar, T.J.A. S, D.C.R. Espinosa, Application of Advanced Oxidative Process for Organic Compounds Removal from Bayer Liquor Minerals, Metals Mater. Ser., (2020) 60-64.
[3] M.A.S. Pastor, A.B. Botelho Junior, D.C.R. Espinosa, J.A.S. Tenório, M.D.P.G.J.O. S. Baltazar, Application of Advanced Oxidation Process Using Ozonation Assisted with Hydrogen Peroxide for Organic Compounds Removal from Bayer Liquor, Ozone: Sci. Eng. (2021) 1–11.
[4] C. Sato, Y. Yamada, Y. Shibue, A. Sakamoto, N.J.L.M. Arakawa, New process for removal of organics from Bayer liquor, (1982) 119-128.
[5] J. Guthrie, W. Imbrogno, Characterization of organics in Bayer liquor, in: Essential Readings in Light Metals, Springer, 2016, pp. 268-277.
[6] E.S. Beach, J.L. Duran, C.P. Horwitz, T.J.J.I. Collins, Activation of hydrogen peroxide by an Fe-TAML complex in strongly alkaline aqueous solution: homogeneous oxidation catalysis with industrial significance, Ind. Eng. Chem. Res. 48 (2009) 7072–7076.
[7] P. Wu, G. Liu, X. Li, Z. Peng, Q. Zhou, T. Qi, Y. Wang, L. Shen, Removal of organics from Bayer liquors via foam flotation, J. Cleaner Prod. 130353 (2022).
[8] M.A. Wellington, Effect of thermal treatment of bauxite ore on carbon (organic and inorganic) content and solubility in Bayer process liquor, Ind. Eng. Chem. Res. 52 (2013) 1434–1438.
[9] E.-W. Song, D.-Z. Han, L.-J. Qi, F.-J. Zhou, The Study of TCA Applied in Organic Removal from Sodium Aluminate Solution, in: Light Metals 2021, Springer, 2021, pp. 18–23.
[10] Z. Zhao, Y. Yang, Y. Xiao, Y. Fan, Recovery of gallium from Bayer liquor: A review, Hydrometallurgy 125 (2012) 115–124.
[11] G. Lever, Removal of oxalate from Bayer process liquor, in, Google Patents, 1981.
[12] G.-H. Liu, W.-B. Dong, T.-G. Qi, Q.-S. Zhou, Z.-H. Peng, X.-B. Li, Behavior of calcium oxalate in sodium aluminate solutions, Trans. Nonferrous Metals Soc. China 27 (2017) 1878–1887.
[13] D. Fernández, I. Robles, F.J. Rodríguez-Valadez, L.A. Godínez, Novel arrangement for an electro-Fenton reactor that does not require addition of iron, acid and a final neutralization stage, Towards the development of a cost-effective technology for the treatment of wastewater, Chemosphere 199 (2018) 251–255.
[14] J. Ji, R.M. Aleisa, H. Duan, J. Zhang, Y. Yin, M. Xing, Metallic active sites on MoO_2 (110) surface to catalyze advanced oxidation processes for efficient pollutant removal, Iscience 23 (2020), 100861.
[15] F. Valeriani, L.M. Margarucci, V. Romano Spica, Recreational use of spa thermal waters: criticisms and perspectives for innovative treatments, Int. J. Environ. Res. Public Health, 15 (2018) 2675.
[16] J.S.C. Loh, G.M. Brodie, G. Power, C.F. Vernon, Wet oxidation of precipitation yield inhibitors in sodium aluminate solutions: Effects and proposed degradation mechanisms, Hydrometallurgy 104 (2010) 278–289.
[17] Z. Liu, W. Li, W. Ma, Z. Yin, G. Wu, Conversion of sulfur by wet oxidation in the bayer process, Metall. Mater. Trans. B 46 (2015) 1702–1708.
[18] A. Hassani, S. Krishnan, J. Scaria, P. Eghbali, P. Nidheesh, Z-scheme photocatalysts for visible-light-driven pollutants degradation: a review on recent advancements, Curr. Opin. Solid State Mater. Sci. 25 (2021), 100941.
[19] A. Fernandes, D. Santos, M. Pacheco, L. Ciríaco, A. Lopes, Electrochemical oxidation of humic acid and sanitary landfill leachate: influence of anode material, chloride concentration and current density, ScTEn 541 (2016) 282–291.
[20] T.N. Weerasinghe Mohottige, M.P. Ginige, A.H. Kaksonen, R. Sarukkalige, K. Y. Cheng, Rapid start-up of a bioelectrochemical system under alkaline and saline conditions for efficient oxalate removal, Bioresour. Technol. 250 (2018) 317–327.
[21] F. Ghanbari, F. Zirrahi, K.-Y.A. Lin, B. Kakavandi, A. Hassani, Enhanced electro-peroxone using ultrasound irradiation for the degradation of organic compounds: A comparative study, J. Environ. Chem. Eng. 8 (2020), 104167.
[22] C. Shi, X. Zhang, X. Zhang, P. Chen, L. Xu, Ultrasonic desulfurization of amphiphilic magnetic-Janus nanosheets in oil-water mixture system, Ultrason. Sonochem. 76 (2021), 105662.
[23] N. Wang, T. Zheng, G. Zhang, P. Wang, A review on Fenton-like processes for organic wastewater treatment, J. Environ. Chem. Eng. 4 (2016) 762–787.
[24] A. Hassani, M. Malhotra, A.V. Karim, S. Krishnan, P. Nidheesh, Recent progress on ultrasound-assisted electrochemical processes: A review on mechanism, reactor strategies, and applications for wastewater treatment, Environ. Res. 205 (2022), 112463.
[25] M.R.K. Kashani, R. Kiani, A. Hassani, A. Kadier, S. Madihi-Bidgoli, K.-Y.A. Lin, F. Ghanbari, Electro-peroxone application for ciprofloxacin degradation in aqueous

solution using sacrificial iron anode: A new hybrid process, Separ. Purif. Technol. 292 (2022), 121026.
[26] G. Boczkaj, A. Fernandes, Wastewater treatment by means of advanced oxidation processes at basic pH conditions: a review, Chem. Eng. J. 320 (2017) 608–633.
[27] N. Lu, X.-F. Wu, J.-Z. Zhou, X. Huang, G.-J. Ding, Bromate oxidized from bromide during sonolytic ozonation, Ultrason. Sonochem. 22 (2015) 139–143.
[28] V. Naddeo, V. Belgiorno, D. Ricco, D. Kassinos, Degradation of diclofenac during sonolysis, ozonation and their simultaneous application, Ultrason. Sonochem. 16 (2009) 790–794.
[29] H. He, Y. Liu, S. You, J. Liu, H. Xiao, Z. Tu, A review on recent treatment technology for herbicide atrazine in contaminated environment, Int. J. Environ. Res. Public Health 16 (2019) 5129.
[30] A. Fernandes, P. Makoś, Z. Wang, G. Boczkaj, Synergistic effect of TiO_2 photocatalytic advanced oxidation processes in the treatment of refinery effluents, Chem. Eng. J. 391 (2020), 123488.
[31] A. Fernandes, M. Gągol, P. Makoś, J.A. Khan, G. Boczkaj, Integrated photocatalytic advanced oxidation system (TiO_2/UV/O_3/H_2O_2) for degradation of volatile organic compounds, Separ. Purif. Technol. 224 (2019) 1–14.
[32] K.S. Suslick, Sonochemistry, Sci 247 (1990) 1439–1445.
[33] M.P. Rayaroth, C.T. Aravindakumar, N.S. Shah, G. Boczkaj, Advanced oxidation processes (AOPs) based wastewater treatment-unexpected nitration side reactions-a serious environmental issue: A review, Chem. Eng. J. 430 (2022), 133002.
[34] K. Fedorov, K. Dinesh, X. Sun, R.D.C. Soltani, Z. Wang, S. Sonawane, G. Boczkaj, Synergistic effects of hybrid advanced oxidation processes (AOPs) based on hydrodynamic cavitation phenomenon–a review, Chem. Eng. J. 134191 (2021).
[35] K. Fedorov, X. Sun, G. Boczkaj, Combination of hydrodynamic cavitation and SR-AOPs for simultaneous degradation of BTEX in water, Chem. Eng. J. 417 (2021), 128081.
[36] K. Fedorov, M. Plata-Gryl, J.A. Khan, G. Boczkaj, Ultrasound-assisted heterogeneous activation of persulfate and peroxymonosulfate by asphaltenes for the degradation of BTEX in water, J. Hazard. Mater. 397 (2020), 122804.
[37] W.-Q. Guo, R.-L. Yin, X.-J. Zhou, J.-S. Du, H.-O. Cao, S.-S. Yang, N.-Q. Ren, Sulfamethoxazole degradation by ultrasound/ozone oxidation process in water: kinetics, mechanisms, and pathways, Ultrason. Sonochem. 22 (2015) 182–187.
[38] M. Cui, M. Jang, S.-H. Cho, D. Elena, J. Khim, Enhancement in mineralization of a number of natural refractory organic compounds by the combined process of sonolysis and ozonolysis (US/O_3), Ultrason. Sonochem. 18 (2011) 773–780.
[39] A. Weissler, H.W. Cooper, S. Snyder, Chemical effect of ultrasonic waves: oxidation of potassium iodide solution by carbon tetrachloride, J. Am. Chem. Soc. 72 (1950) 1769–1775.
[40] S. Koda, T. Kimura, T. Kondo, H. Mitome, A standard method to calibrate sonochemical efficiency of an individual reaction system, Ultrason. Sonochem. 10 (2003) 149–156.
[41] M. Kuijpers, M. Kemmere, J. Keurentjes, Calorimetric study of the energy efficiency for ultrasound-induced radical formation, Ultra 40 (2002) 675–678.
[42] Y. Rao, H. Long, J. Hao, The oxidative degradation of Caffeine in UV/Fe (II)/persulfate system—Reaction kinetics and decay pathways, Water Environ. Res. 93 (2021) 559–569.
[43] Y. Zhang, S. Yin, H. Li, J. Liu, S. Li, L. Zhang, Treatment of ammonia-nitrogen wastewater by the ultrasonic strengthened break point chlorination method, J. Water Process Eng. 45 (2022), 102501.
[44] R. Kidak, N. Ince, Catalysis of advanced oxidation reactions by ultrasound: A case study with phenol, J. Hazard. Mater. 146 (2007) 630–635.
[45] L.K. Weavers, Sonolytic ozonation for the remediation of hazardous pollutants, Adv. Sonochem. (2001) 111.
[46] D. Kanakaraju, B.D. Glass, M. Oelgemöller, Advanced oxidation process-mediated removal of pharmaceuticals from water: a review, J. Environ. Manage. 219 (2018) 189–207.
[47] O. Legrini, E. Oliveros, A. Braun, Photochemical processes for water treatment, Chem. Rev. 93 (1993) 671–698.
[48] G. Power, J. Loh, Organic compounds in the processing of lateritic bauxites to alumina: Part 1: Origins and chemistry of organics in the Bayer process, Hydrometallurgy 105 (2010) 1–29.
[49] S. Fang, W. Wang, S. Tong, C. Zhang, P. Liu, Evaluation of the effects of isolated lignin on cellulose enzymatic hydrolysis of corn stover pretreatment by NaOH combined with ozone, Molecules 23 (2018) 1495.
[50] L.K. Weavers, F.H. Ling, M.R. Hoffmann, Aromatic compound degradation in water using a combination of sonolysis and ozonolysis, EnST 32 (1998) 2727–2733.
[51] T. Sivasankar, V.S. Moholkar, Mechanistic features of the sonochemical degradation of organic pollutants, AIChE 54 (2008) 2206–2219.
[52] E.B. Flint, K.S. Suslick, The temperature of cavitation, Sci 253 (1991) 1397–1399.
[53] N. Ince, G. Tezcanli, R. Belen, İ.G. Apikyan, Ultrasound as a catalyzer of aqueous reaction systems: the state of the art and environmental applications, Appl. Catal. B 29 (2001) 167–176.
[54] L. Wang, X. Lan, W. Peng, Z. Wang, Uncertainty and misinterpretation over identification, quantification and transformation of reactive species generated in catalytic oxidation processes: A review, J. Hazard. Mater. 408 (2021), 124436.
[55] G. Le Truong, J. De Laat, B. Legube, Effects of chloride and sulfate on the rate of oxidation of ferrous ion by H2O2, Water Res. 38 (2004) 2384–2394.
[56] M. Gągol, E. Cako, K. Fedorov, R.D.C. Soltani, A. Przyjazny, G. Boczkaj, Hydrodynamic cavitation based advanced oxidation processes: Studies on specific effects of inorganic acids on the degradation effectiveness of organic pollutants, J. Mol. Liq. 307 (2020), 113002.
[57] M. Yan, D. Dryer, G.V. Korshin, Spectroscopic characterization of changes of DOM deprotonation–protonation properties in water treatment processes, Chemosphere 148 (2016) 426–435.
[58] M. Mischopoulou, P. Naidis, S. Kalamaras, T. Kotsopoulos, P. Samaras, Effect of ultrasonic and ozonation pretreatment on methane production potential of raw molasses wastewater, Renewable Energy 96 (2016) 1078–1085.
[59] P.G. Coble, S.A. Green, N.V. Blough, R.B. Gagosian, Characterization of dissolved organic matter in the Black Sea by fluorescence spectroscopy, Nature 348 (1990) 432–435.
[60] K.M. Elkins, D.J. Nelson, Spectroscopic approaches to the study of the interaction of aluminum with humic substances, Coord. Chem. Rev. 228 (2002) 205–225.
[61] Z. He, S. Song, H. Zhou, H. Ying, J. Chen, C.I. Reactive Black 5 decolorization by combined sonolysis and ozonation, Ultrason. Sonochem. 14 (2007) 298–304.
[62] M.A. Oturan, J. Pinson, Hydroxylation by electrochemically generated OH. bul. radicals. Mono-and polyhydroxylation of benzoic acid: Products and isomer distribution, J. Phys. Chem. 99 (1995) 13948–13954.
[63] N.N. Mahamuni, Y.G. Adewuyi, Advanced oxidation processes (AOPs) involving ultrasound for waste water treatment: a review with emphasis on cost estimation, Ultrason. Sonochem. 17 (2010) 990–1003.